JOURNAL OF APPLIED ELECTROCHEMISTRY 14 (1984) 177–186

Hypochlorite electro-generation. I. A parametric study of a parallel plate electrode cell

G. H. KELSALL*

Electricity Council Research Centre, Capenhurst, Chester, CH1 6ES, UK

Received 29 March 1983

A parametric study is described of a parallel plate $Ti/PbO_2/x$ mol dm^{-3} NaCl/Ti hypochlorite cell, for which the cell voltage, current efficiency, and energy yield (mol ClO^- kW h^{-1}) were examined as functions of current density, chloride concentration, and electrolyte flow rate, inlet temperature and pH.

The cell was found to behave ohmically, with current efficiencies of 85–99% for 0.5 mol dm^{-3} NaCl electrolyte, a typical chloride concentration for sea water. However, the hypochlorite energy decreased substantially with increased current density, reflecting the large contribution of the electrolyte ohmic potential drop to the cell voltage.

The behaviour of the Ti/PbO_2 anode was found to be irreproducible, and low temperature (say $\leqslant$ 278 K)/high current density operation was irreversibly detrimental both in terms of the anode potential/cell voltage and current efficiency.

Nomenclature

b	polarization resistance (ohm m^2)
d_{min}	interelectrode spacing to minimize the cell voltage (m)
$f(x)$	volume fraction of gas at level x
f_{av}	average volume fraction of gas
F	Faraday constant (96487 C mol^{-1})
h	electrode length/height (m)
$i(x)$	current density at position x (A m^{-2})
i_{av}	average current density (A m^{-2})
I	cell current (A)
P	pressure of gas evolved at electrodes (N m^{-2})
R	universal gas constant (8.314 J mol^{-1} K^{-1})
R_{eff}	total ohmic resistance of electrolyte and gas in cell (ohm)
s	bubble rise rate (m s^{-1})
t_{Cl^-}	chloride ion transport number
T	electrolyte temperature (K)
w	electrode width (m)
x	distance from bottom of electrodes (m)
z	number of Faradays per mole of gas evolved
$\eta(x)$	overpotential at position x (V)
ρ	resistivity of gas free electrolyte (ohm m)
$\rho(x)$	resistivity at level x of electrolyte containing bubbles (ohm m)

1. Introduction

Interest in the local electrogeneration of chlorine and hypochlorite has increased dramatically in recent years [1], because of the potential dangers of transporting, storing and handling large volumes of liquid chlorine, highlighted by several recent near disasters. As one of the largest users of chlorine as a biocide in cooling waters, the UK electricity supply industry in particular would have to provide itself with an alternative source in the event of chemical companies such as ICI, being forced by UK Government or EEC regulations, to restrict the supply of bulk liquid chlorine.

The in-house production alternative involves two options:

i. chlorine generation in a miniature chloralkali cell, probably incorporating a membrane and using a purified brine anolyte, and
ii. hypochlorite ($HClO + ClO^-$) generation in an undivided cell, in which the anodically evolved

* Present address: Department of Mineral Resources Engineering, Imperial College, London, SW7 2BP, UK.

0021-891X/84 $03.00 + .12

chlorine is hydrolysed in an anode reaction layer, and which uses either brine, or sea water electrolyte where available. However, in this case, the maximum attainable hypochlorite concentration is limited by loss reactions, due to its oxidation and reduction.

As both the capital cost and the energy yield (mol Cl_2 $kW\,h^{-1}$) for the former cell are likely to be greater than for the latter, the choice will depend, *inter alia*, on the required scale of production.

The literature on hypochlorite electrogeneration has been reviewed previously [2, 3], from which it was evident that little had been published on the 'single pass' mode of cell operation. Most authors had chosen to study recirculating systems, where the compositional change per pass was small. The purpose of the presently reported work was to quantify the effect of experimental variables on the 'single pass' performance of a small parallel plate hypochlorite cell, prior to the construction of a scaled-up device. The influence of electrode length was not determined, since the problem had already been modelled, at least in terms of the general effect of gas bubbles on the electrolyte resistivity, current density distribution and the inter-electrode spacing to minimize the cell voltage [4, 5].

2. Electrochemistry and chemistry of the Cl_2–NaCl–H_2O system

Primary reactions:

$$\text{Anode: } 2Cl^- \rightarrow Cl_2 + 2e^- \quad (1)$$

$$\text{Cathode: } 2H_2O + 2e^- \rightarrow 2OH^- + H_2 \quad (2)$$

$$\text{Solution: } Cl_2 + H_2O \rightarrow HClO + Cl^- + H^+ \quad (3)$$

$$HClO \rightleftharpoons H^+ + ClO^- \quad (4)$$

Loss reactions:

$$\text{Anode: } 6ClO^- + 3H_2O \rightarrow 2ClO_3^- + 4Cl^- + 6H^+ + 3/2O_2 + 6e^- \quad (5)$$

$$2H_2O \rightarrow O_2 + 4H^+ + 4e^- \quad (6)$$

$$\text{Cathode: } ClO^- + H_2O + 2e^- \rightarrow Cl^- + 2OH^- \quad (7)$$

$$\text{Solution: } 2HClO + ClO^- \rightarrow ClO_3^- + 2Cl^- + 2H^+ \quad (8)$$

$$2ClO^- \rightarrow O_2 + 2Cl^- \quad (9)$$

Other possible loss reactions which may normally be neglected in a well designed hypochlorite cell are:

i. anodic hydrogen oxidation – limited by hydrogen solubility in the electrolyte

ii. anodic oxidation of ClO_3^- to ClO_4^- – limited by the low concentration of ClO_3^-, which ought ideally to be absent

iii. cathodic reduction of O_2, ClO_3^- and ClO_4^-

iv. reduction of ClO^- by hydrogen, which should be disengaged from the cell efflux to minimize this reaction

3. Cell design considerations

The primary reactions 1 and 2 are charge transfer controlled at least at high chloride concentrations, whereas the loss reactions 5 and 7 are usually mass transport controlled [6, 7]. To minimize the cell voltage/ohmic potential drops in the electrolyte, a narrow interelectrode gap is required, and with gas evolution, relatively high mass transport rates to both electrodes are likely.

This is exacerbated by the need for a high linear electrolyte velocity to reduce gas locking, promote more uniform current density distribution [4, 5] and to reduce undue cathode precipitate growth in the presence of calcium and magnesium salts from hard natural water or sea water. However, Kuhn *et al.* [8] have shown that inhibition of hypochlorite cathodic reduction is achieved by these $Mg(OH)_2$ and $Ca(OH)_2$ films, or by operation with a large anode to cathode area ratio [9].

The effect of the high mass transport rate regime will depend on whether the cell is operated in single pass or recycle mode. With a sea water electrolyte, the low chloride conversion and low efflux hypochlorite concentration of single pass operation could be tolerated, and an increased flow rate will decrease the rate of loss reactions, at constant efflux hypochlorite concentration. However, when a brine electrolyte is used, the significant cost of salt requires either the cell to be operated in recycle mode or the use of a cascade of cells, to optimize salt conversion with respect to the apparent energy requirement for hypochlorite generation. In this configuration the rates of the mass transport controlled loss reactions become

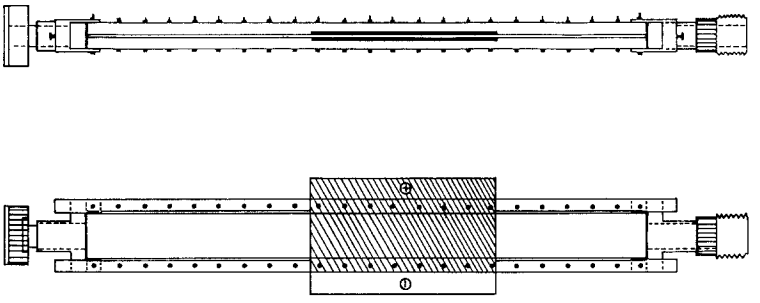

Fig. 1. Parallel plate hypochlorite cell.

increasingly significant, since they are linearly dependent on the hypochlorite concentration. Consequently, a maximum is observed in the concentration–time profile [10]; zero apparent current efficiency occurs at the maximum, when the charge transfer controlled formation reaction rate is equal to the mass transport controlled loss reaction rate. Depletion of the chloride reactant causes a decrease in hypochlorite concentrations at longer times (i.e. negative apparent current efficiencies).

Originally, the intention was to carry out a partial factorial experiment, to quantify the main effects and interactions of the experimental variables by regression analysis, yielding an equation describing the behaviour of the cell. However, this was precluded by the irreproducible behaviour of the Ti/PbO_2 anode, which will be reported in Part II of these papers. Part III will cover the engineering/cell design aspects of hypochlorite generation.

4. Experimental details

A plane parallel plate flow cell was chosen as the simplest design, and because mass transport correlations exist for such rectangular flow channels [11], including corrections for the effects of gas evolution [12]. From a range of possible anode materials with a high oxygen and low chlorine overpotential (Ti/Pt, $Ti/Pt–Ir$, Ti/RuO_2, etc.), an electrodeposited PbO_2 on Ti anode was chosen, accepting its higher chlorine overpotential compared with Ti/RuO_2, but considerably lower capital cost. As the loss of Pt from Ti/Pt had been reported [2] as a major problem with early hypochlorite cells, the possibility of *in situ* replating of worn PbO_2 was an additional consideration. Titanium itself was chosen as the cathode, having excellent corrosion resistance at rest potential in brine/sea water, and an acceptable hydrogen overpotential [13, 14], with the formation of a TiH_x surface phase. Clearly the cathode overpotential/cell voltage could have been lowered significantly by using say steel, but its corrosion at rest potential would produce iron hydroxides which could then be transported to, and deposited on the anode.

The cell shown in Fig. 1, incorporated a $200 \times 50\,mm^2$ Ti (IMI type 115) cathode and Ti/PbO_2 anode (Appendix A), with hydrodynamic entry (0.25 m) and exit (0.15 m) lengths calculated from data published by Pickett and Ong [15]. The electrolyte flow circuit was built of 20 mm i.d. uPVC tubing and valves (G. Fisher Ltd), and included a magnetically coupled pump (Iwaki MD80) with polypropylene contact surfaces and ceramic shaft, so that no corrodible materials were in contact with the electrolyte. Deionised water (Elga B2000/C800 deioniser) was used to make up $1\,m^3$ of sodium chloride electrolyte (BDH Analar grade) in a PVC glass fibre reinforced tank. An EIL 7030 pH meter, with temperature compensator was used to monitor the electrolyte pH, adjustments being made by HCl or NaOH additions. Regulation of the electrolyte temperature was achieved by 3×3 kW silica bar heaters (Thermal Syndicate Ltd) and a cooling unit (F and R Cooling Ltd Model RCU 3) linked to a QVF heat exchanger (HE6/10). Measurement of the electrolyte temperature at the cell inlet and outlet was by platinum resistance thermometers (Sensing Devices Ltd) connected to a (Solartron) $100\,\mu A$ power supply. The electrolyte flow rate was monitored by a PTFE venturi device linked hydraulically to a differential pressure sensor and associated electronics (Tekflo Ltd) to give a digital display of flow rate, and a corresponding analogue output voltage.

Constant current was fed to the cell from a

50 A/60 V power supply (Farnell Ltd), and a data logger (Solartron Compact 33) was used to monitor the current, cell voltage electrode potentials, pH, flow rate, and electrolyte temperature. Fine PTFE tubing inserted through the side of the 3 mm thick PVC interelectrode spacer, was used for Luggin probes in the determination of the electrode potentials.

The cell was operated in single pass mode to minimize complications due to the loss Reactions 5 and 7, and a sample of the efflux taken from each set of operating conditions. The analytical method used for the determination of the hypochlorite concentration is given in Appendix B; a full product analysis was not attempted because of the low chloride conversion and the large number of samples involved. The hypochlorite current efficiency and energy yield (mol ClO^- $kW\,h^{-1}$) could be determined with an estimated error of ± 6%, the two main sources of error being in the analysis (± 4%) and in the measurement of the flow rate (± 2%).

5. Results and discussion

Fig. 2 shows a typical set of cell voltage/current density data, taken after a prepolarization period (⩾ 300 s), for various flow rates, chloride concentrations, electrolyte inlet temperature, and interelectrode gaps. For current densities envisaged in a practical hypochlorite cell, say ⩾ 1 $kA\,m^{-2}$, the cell behaved ohmically, with higher apparent resistance for lower temperatures and flow rates, due to the latter's influence on the gas concentration in the interelectrode gap and its consequent effect on the effective electrolyte resistivity. The effect of changing the NaCl concentration or interelectrode gap, was again to change the electrolyte ohmic potential drop and so the cell voltage, as shown in Fig. 2.

Nagy [5], following Tobias [4], derived the following equation for the effective electrolyte resistance, allowing for the presence of the electrogenerated bubbles creating voidage:

$$R_{\text{eff}} = \frac{2RT\rho I}{hw^2PzFs} \frac{1}{f_{\text{av}}(1-f_{\text{av}})(2-f_{\text{av}})^2} \quad (10)$$

This equation gives typical values of 0.07 Ω for the range of conditions given in Fig. 2, compared with values of ~ 0.1 Ω taken from the data in Fig. 2, which includes the electrode polarization

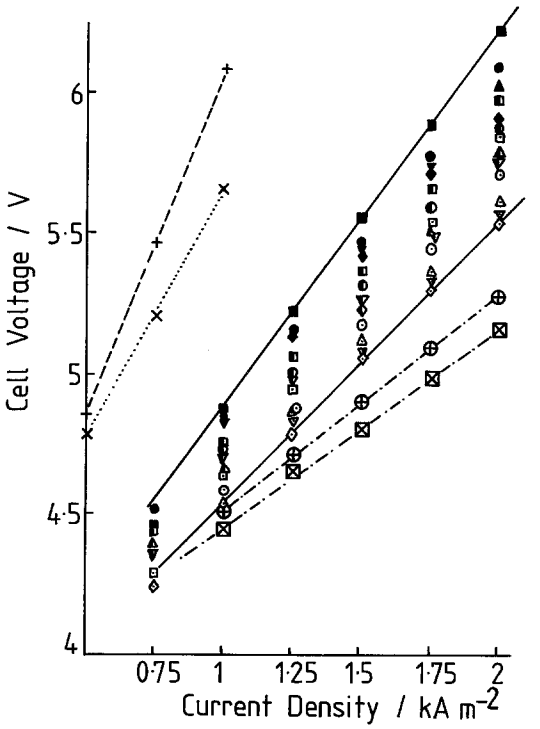

Fig. 2. Cell voltage/current density relationships. (–) 3 mm gap, 0.5 mol dm^{-3} NaCl: ▫ 0.25, ○ 0.5, △ 1, ▽ 2, ◇ 3 $dm^3\,min^{-1}$, 293 K; ◧ 0.25, ◐ 0.5, ▲ 1, ▼ 2, ◆ 3 $dm^3\,min^{-1}$, 288 K; ■ 0.25, ● 0.5, ▲ 1, ▼ 2, ◆ 3 $dm^3\,min^{-1}$, 283 K. (–·–·–) ⊕ 0.8 mm gap, 0.5 mol dm^{-3} NaCl, 288 K, 0.5 $dm^3\,min^{-1}$; ⊠ 0.8 mm gap, 0.5 mol dm^{-3} NaCl, 288 K, 2 $dm^3\,min^{-1}$. (. . .) × 3 mm gap, 0.3 mol dm^{-3} NaCl, 288 K, 1 $dm^3\,min^{-1}$. (– – –) + 1.5 mm gap, 0.1 mol dm^{-3} NaCl, 288 K, 1 $dm^3\,min^{-1}$.

terms. To avoid generating nonlinear differential equations, the model [4, 5] assumed linear electrode polarization:

$$\eta(x) = b \cdot i(x) \quad (11)$$

By differentiating Equation 10, R_{eff} was shown to assume a minimum value when $f_{\text{av}} = 0.36$, with little voltage benefit in operating with $f_{\text{av}} \geqslant 0.2$ [4]. The interelectrode gap at which the cell voltage was minimized, was derived [5] as:

$$d_{\text{min}} = 1.69 \frac{RT}{PzF} \frac{i_{\text{av}}}{s} \cdot h \quad (12)$$

Assuming that the bubble rise rate is approximately equal to the electrolyte phase velocity [31], when the latter is 0.5 $dm^3\,min^{-1}$ Equation 12 predicts a minimum voltage for $d_{\text{min}} \cong 1.5$ mm at 2 $kA\,m^{-2}$. However, the model [4, 5] strictly applies to natural/gas induced convection conditions and not to pumped flow [31], so that lower voltages were observed with a 0.8 mm gap.

The nonlinear relationship, of the type derived by Tobias *et al.* [16, 17]:

$$\rho(x) = \rho[1-f(x)]^{-1.5} \qquad (13)$$

between the local effective resistivity $\rho(x)$ of an electrolyte with bulk resistivity ρ, due to a local gas bubble fraction $f(x)$ at an electrode height x, evidently did not give rise to nonohmic behaviour over the range of current/flow rate ratios studied here. The distorted current density distribution due to the presence of gas bubbles in the electrolyte [4, 5], was probably responsible for the apparently ohmic behaviour, with the nonlinear components of the current/overpotential relationship and the electrolyte resistance (Equation 10) cancelling. Tobias' model [4] indicated that although the gas fraction in the electrolyte might vary typically (for the present case) from 0 to 50% from cell inlet to outlet, the levelling effect of the electrode overpotentials causes the local current density to vary between only 110 and 90% of its average value over the same distances. However, there is clearly a voltage penalty in scaling-up a single electrode in the direction of electrolyte/gas flow, which should be avoided/minimized by judicious cell design.

For current densities $\leqslant 0.75\,\mathrm{kA\,m^{-2}}$, the apparent cell resistance (i.e. the slope of the cell voltage/current relationship), was greater than for $\geqslant 0.75\,\mathrm{kA\,m^{-2}}$ and nonohmic, presumably due mainly to the increase to some quasi steady-state value of the concentration of gas bubbles on the electrode surfaces.

The polarization behaviour of a Ti/PbO_2 anode and Ti cathode, again after a prepolarization period of $\geqslant 300$ s, is shown in Figs. 3a and b respectively. The non-Tafel behaviour of the anode above $\approx 100\,\mathrm{A\,m^{-2}}$ is unlikely to result from slow mass transport of chloride ions as the anode potentials were flow rate independent. Also, using the correlations of Pickett and Ong [15], the lowest flow rate used gives a calculated convective–diffusion limited current density of $1027\,\mathrm{A\,m^{-2}}$, even without migrational and bubble-induced enhancement. This figure assumes a chloride concentration of $0.5\,\mathrm{mol\,dm^{-3}}$ since the depletion was only 0.1–2.5% in single pass operation. The migrational contribution could increase this current density by a factor of $(1-t_{Cl^-})^{-1}$, where the chloride ions transport number, t_{Cl^-}, is 0.62 [18],

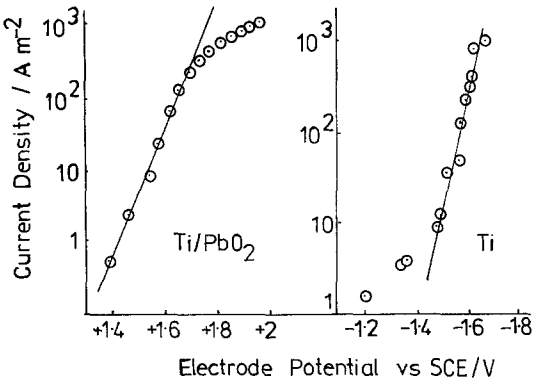

Fig. 3. (a) Ti/PbO_2 anode polarization in $0.5\,\mathrm{mol\,dm^{-3}}$ NaCl. (b) Ti cathode polarization in $0.5\,\mathrm{mol\,dm^{-3}}$ NaCl.

although this is not rigorously correct since t_{Cl^-} is defined under conditions where no concentration gradients exist, and Ohm's law applies.

The cathodically generated hydrogen bubbles also enhance the transport rate, primarily due to the increased electrolyte linear velocity caused by the void fraction created by the gas [19]. However, the gas distribution in the electrolyte depends on the current density distribution. Tobias [4] gives data for the local electrolyte void fraction as a function of electrode height and mean current density, this can be used to estimate local electrolyte phase Reynolds numbers and hence local mass transport rates from suitable correlations [11].

With the highest current (20 A) and lowest electrolyte flow rate used ($0.5\,\mathrm{dm^3\,min^{-1}}$), the mean electrolyte void fraction due to gas was $\approx 30\%$, using a figure of $\approx 7 \times 10^{-4}\,\mathrm{mol\,dm^{-3}}$ for the solubility of hydrogen, and neglecting the minor effects of hydrostatic pressure and the average gas volume resident on the electrode surface, which probably cancel. There is the additional effect due to oxygen evolved at the anode by Reactions 5 and 6, though under the conditions used, the current efficiency loss to these reactions is very low (see Fig. 5). The combination of the bubble and migrational effects is to enhance the convective–diffusion limited current density ($\approx 1\,\mathrm{kA\,m^{-2}}$) by a factor of say three, so that deviation from Tafel behaviour above $\sim 0.1\,\mathrm{kA\,m^{-2}}$ (Fig. 3a) cannot be attributed to slow Cl^- mass transfer.

By contrast with the Ti/PbO_2 anode, using a similar Luggin probe, the hydrogen evolving Ti cathode showed Tafel behaviour (see Fig. 3b)

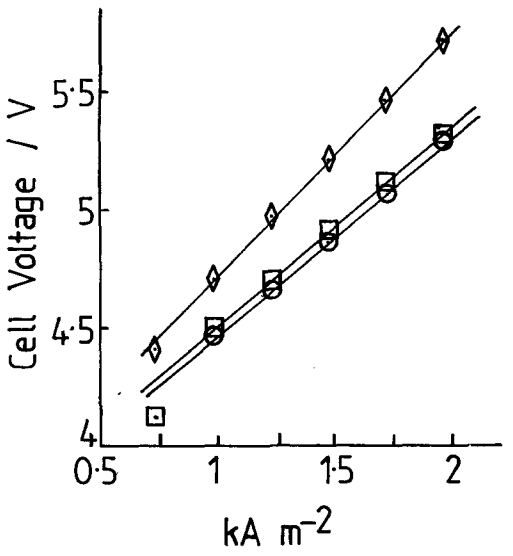

Fig. 4. Cell voltage/current density relationships for Ti/PbO_2 anodes in 0.5 mol dm^{-3} NaCl, 1.5 mm gap, 0.5 $dm^3 min^{-1}$, 283 K. Anodes plated at 1 kA m^{-2} ⊙ 343 K, ⊡ 323 K, ◇ 343 K after operation at 278 K.

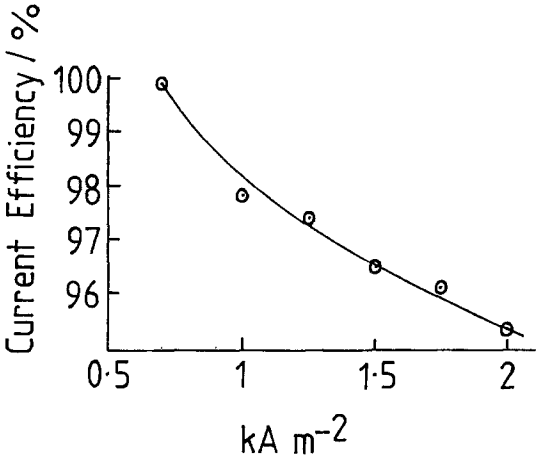

Fig. 5. Current efficiency/current density relationship for 0.5 mol dm^{-3} NaCl, 1.5 mm gap, 0.5 $dm^3 min^{-1}$, 288 K.

for currents $\geqslant 10$ A m^{-2}, and with time formed a black surface phase, established by X ray diffraction to be $TiH_{1,94}$. Uncompensated ohmic potential loss between the anode surface and its Luggin probe tip was therefore unlikely to cause the non-Tafel behaviour of the anode. This may have been due to solid state potential loss, resulting from the growth of a resistive oxide layer between the Ti substrate and PbO_2 deposit, as has been postulated for Ti/MnO_2 [20], Ti/RuO_2 [21] and Ti/Fe_3O_4 [22].

More recently however, the loss in activity of the Ti/PbO_2 anode in sulphuric acid has been ascribed to the consumption of active sites such as Pb^{3+} in the nonstoichiometric PbO_2, coupled to a slow solid state diffusion from the bulk PbO_2 to the solution interface [23]. However, this model does not account for the differences between Ti and Pt (or Ti/Pt) substrates in the rates of loss of activity of the composite anodes [24]. Reactivation was observed on removing and then replacing the electrode in the acid electrolyte, followed by decay back to the original behaviour. This was not observed in the present work in chloride solutions, in which irreversible deactivation was found at high current densities/potentials and low temperatures (say $\leqslant 278$ K), which could occur in winter at coastal hypochlorite plants using sea water electrolytes. The effect of such thermal treatment is reflected in the differences in the cell voltage/current plots shown in Fig. 4. A more detailed study of Ti/PbO_2 anodes in chloride electrolytes is reported elsewhere [25, 26].

From Fig. 2, for 0.5 mol dm^{-3} NaCl, 3 mm gap, 293 K, 0.5 $dm^3 min^{-1}$ and 2 kA m^{-2}, the cell voltage is ≈ 5.6 V, of which (Fig. 3) ≈ 3.7 V may be ascribed to the thermodynamic voltage (E_{cell}) requirement [30] and the electrode overpotentials, leaving ≈ 1.9 V as a mean ohmic potential loss in the electrolyte ($\approx 34\%$ of the cell voltage). This is in reasonable agreement with the value predicted from Equation 10.

Fig. 5 shows a weak negative dependency of hypochlorite current efficiency on current density. For single pass operation with a 0.5 mol dm^{-3} NaCl electrolyte, the current efficiency was typically 85–100%, depending on the current density, interelectrode gap, flow rate and temperature. Although further oxidation (Reaction 5) or reduction (Reaction 7) of hypochlorite by mass transport from the bulk electrolyte is possible, and recirculation of the electrolyte within the cell would enhance the effect, under the low chloride conversion/low hypochlorite efflux concentration conditions used, the Pickett and Ong mass transport correlation [15] indicates that this is insignificant compared to the experimental errors involved here. However, further oxidation at some higher point on the anode, of hypochlorite formed at some lower point in the anode reaction layer, may

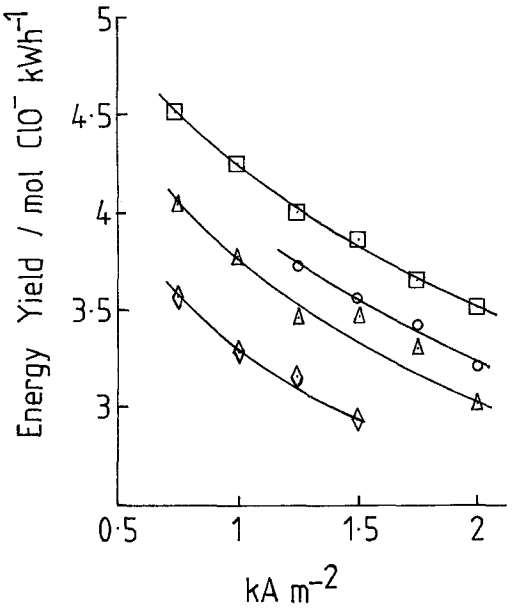

Fig. 6. Energy yield/current density relationships.
▫ 1.5 mm gap, 0.5 mol dm^{-3} NaCl, 0.5 dm^3 min^{-1}, 293 K.
⊙ 1.5 mm gap, 0.5 mol dm^{-3} NaCl, 0.5 dm^3 min^{-1}, 288 K.
△ 1.5 mm gap, 0.5 mol dm^{-3} NaCl, 0.5 dm^3 min^{-1}, 283 K.
◇ 1.5 mm gap, 0.25 mol dm^{-3} NaCl, 0.5 dm^3 min^{-1}, 283 K.

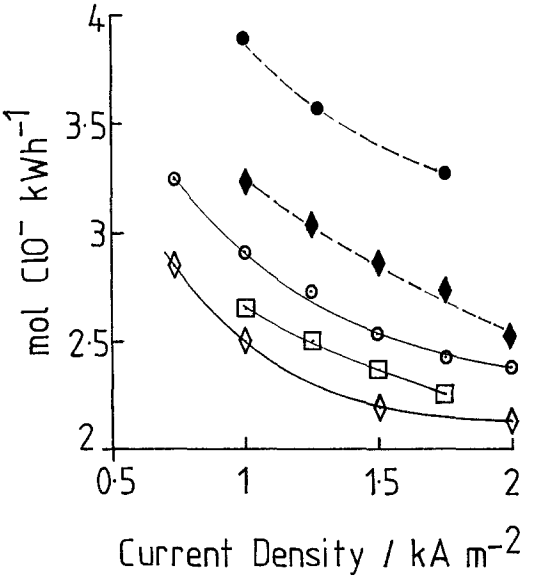

Fig. 7. Energy yield/current density relationships for cell after low temperature operation.
⊙ 0.5 mol dm^{-3} NaCl, 3 mm gap, 0.5 dm^3 min^{-1}, 293 K.
● 0.5 mol dm^{-3} NaCl, 1.5 mm gap, 0.5 dm^3 min^{-1}, 293 K.
▫ 0.5 mol dm^{-3} NaCl, 3 mm gap, 1 dm^3 min^{-1}, 288 K.
◇ 0.5 mol dm^{-3} NaCl, 3 mm gap, 1 dm^3 min^{-1}, 283 K.
♦ 0.5 mol dm^{-3} NaCl, 1.5 mm gap, 1 dm^3 min^{-1}, 283 K.

account for some of the current efficiency loss, though it is not presently possible to quantify the effect, as Ibl and Landolt [6] have pointed out.

After an anode had been subjected to low temperature operation ($\leqslant$ 278 K), the current efficiency in 0.5 mol dm^{-3} NaCl electrolyte was found to decrease to a range of 65–80%, lending support to Gilroy's hypothesis [23] of anode deactivation by active site consumption. The same anode in 0.3 mol dm^{-3} and 0.1 mol dm^{-3} NaCl electrolytes, gave current efficiencies of 47–72% (for 0.5–2 kA m^{-2}) and 34–49% (for 0.5–1 kA m^{-2}) respectively, independent of flow rate. It has been observed with Ti/RuO_2 anodes operated with a sea water electrolyte, which contained an anomalously high manganese ion concentration, that MnO_2 was anodically deposited on the RuO_2, and the hypochlorite current efficiency decreased to zero, as oxygen alone was evolved on this particular form of MnO_2 [27].

As shown in Fig. 6, increasing the current density produced a substantial decrease in the hypochlorite energy yield, due primarily to the electrolyte ohmic potential drop contribution to the cell voltage. A trade-off situation therefore exists between specific energy costs and specific hypochlorite production rate/cell size/cell capital costs; an optimum current density could be calculated if the relationship between cell size and cost could be estimated. Fig. 7 shows energy yield data for the cell/anode subjected to low temperature operation, for which cell voltage/current density data is given in Fig. 4. The differences in the data of the uppermost lines in Figs. 6 and 7, was attributed to the increased anode potential/cell voltage and decreased current efficiency following operation at $\leqslant$ 278 K.

As already discussed, the effect of a decrease in the electrolyte concentration, flow rate or temperature, or of an increase in the interelectrode gap was to increase the electrolyte ohmic potential drop, and hence the cell voltage, as shown in Fig. 2. This is reflected in the energy yield data given in Figs. 6–9, which show as expected, that the greatest hypochlorite energy yield for a given current density, was achieved with a narrow interelectrode gap, and a high NaCl concentration, flow rate and temperature. It should be stressed that

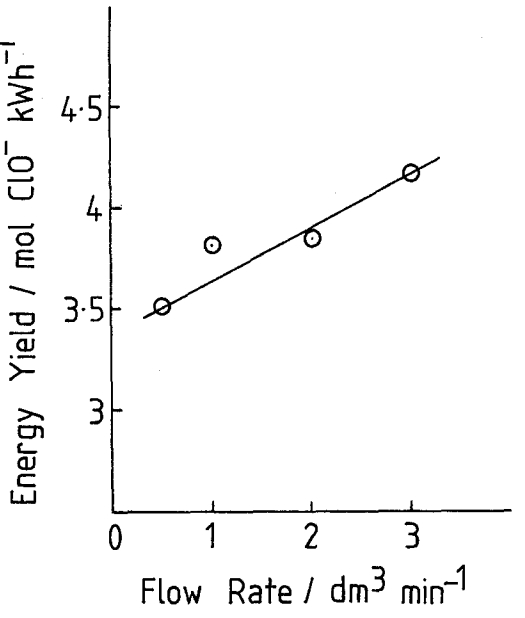

Fig. 8. Energy yield/flow rate relationship
0.5 mol dm^{-3} NaCl, 1.5 kA m^{-2}, 293 K, 1.5 mm gap.

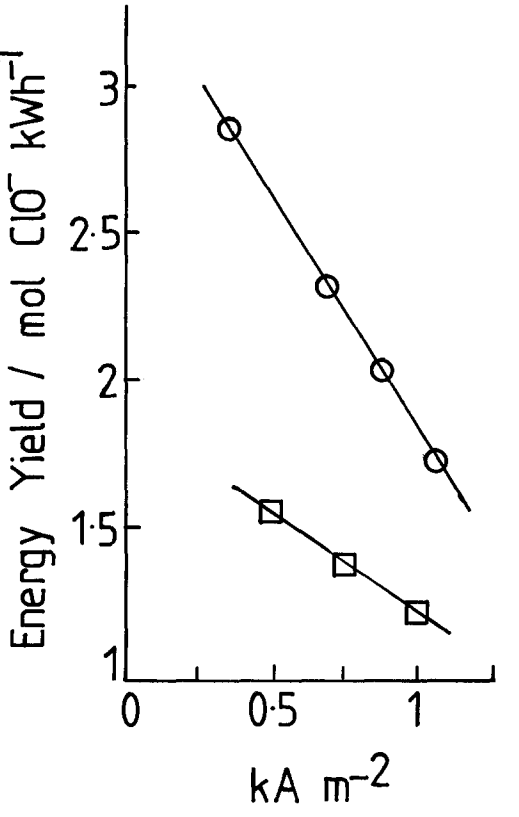

Fig. 9. Energy yield/current density relationship
⊙ 0.3 mol dm^{-3} NaCl, 3 mm gap, 2 $dm^3 min^{-1}$, 278 K.
⊡ 0.1 mol dm^{-3} NaCl, 1.5 mm gap, 0.5 $dm^3 min^{-1}$, 278 K.

this statement refers to single pass operation with low chloride conversion/low hypochlorite efflux concentrations ($\leqslant$ 1000 ppm ClO^- in this work), and would not necessarily apply to recycle operation, when these variables also influence the rate of the hypochlorite loss reactions, as has been shown by Heal *et al.* [10].

The curvature of, for example, the lowest line in Fig. 7, was due to ohmic heating causing an increase in electrolyte temperature from 283 to 289 K in the cell efflux, with a corresponding decrease in the ohmic potential drop – an example of variable interaction. The current also influenced the effective electrolyte conductivity/cell voltage via the electrogeneration of H^+ and OH^- ions. When compared to the bulk electrolyte pH values this produced a lower pH near the anode and a higher pH near the cathode. Hence, for a 0.1 mol dm^{-3} NaCl electrolyte the effect of decreasing the flow rate was to decrease the cell voltage, while the converse was found for 0.5 mol dm^{-3} NaCl, as shown in Fig. 2. For the latter electrolyte, in which the hypochlorite current efficiency was 85–100%, the bulk electrolyte pH over the range 5–11, had no effect on the cell voltage or energy yield.

6. Conclusions

In a $Ti/PbO_2/x$ mol dm^{-3} NaCl/Ti parallel plate flow cell, the hypochlorite current efficiency was found typically to be in the range 85–100%, for 0.5 mol dm^{-3} NaCl electrolyte and current densities $\leqslant$ 2 kA m^{-2}. The effect of an increase in the current density was to produce a significant decrease in the hypochlorite energy yield (mol ClO^- kW h^{-1}), reflecting the large electrolyte ohmic potential drop contribution to the cell voltage.

Low temperature/high current density (i.e. high potential) operation was found to be irreversibly detrimental to the Ti/PbO_2 anode performance, causing an increased potential and decreased current efficiency. Even so, energy yields were achieved of 2.2–4 mol ClO^- kW h^{-1} for 2–1 kA m^{-2}, compared with a range of 3–4.3 mol ClO^- kW h^{-1} with an 'undamaged' anode.

Acknowledgements

The author would like to thank the Electricity Council Research Centre for permission to publish this work, and Mr P. Carrahar for performing the hypochlorite analysis.

Appendix A

Ti/PbO_2 anode preparation

The 200 mm x 100 mm x 2 mm titanium substrate was cleaned/degreased by Analar 1,1,1-trichloroethane (BDH Ltd), and then grit blasted by alumina (Guyson Saftigrain) at 90 psi in a (Guysons Super 4) blasting unit. Loosely adhering particles were removed by compressed air before a final rinse in 1,1,1-trichloroethane. Titanium nuts and bolts were used to make the electrical connection between the Ti current feeder and the electrode, those areas not to be plated then being masked with Lacomit insulant (Cannings Ltd). To avoid undue growth of an air-formed TiO_x film the electrode was transferred as soon as possible following blasting, to the plating cell. This was coupled to a simple flow circuit containing:

$10\ dm^3$ glass aspirator reservoir
Totton Electrics Ltd, PCP 175 magnetically coupled pump
GEC–Elliot 'Rotameter' flow meter with 'Korannite' ceramic float and $\frac{3}{4}$ inch PVC angle seat valve and piping.

The electrolyte, made from (BDH Ltd) Analar grade reagents and deionised water, contained:

$200\ g\ dm^{-3}\ Pb(NO_3)_2$
$10\ g\ dm^{-3}\ Cu(NO_3)_2 \cdot 3H_2O$
$10\ g\ dm^{-3}\ Ni(NO_3)_2 \cdot 6H_2O$
$0.5\ g\ dm^{-3}\ NaF$
$0.5\ g\ dm^{-3}$ Triton-X surfactant

and was preheated (298–343 K) with a silica bar heater (Thermal Syndicate Ltd) immersed in the plating cell. Although PbO_2 deposition was carried out nominally under conditions of charge transfer control, it was found advantageous to use a fluidized bed electrolyte of 0.5–0.6 mm glass beads (Jencons Ltd). This prevented gas bubbles adhering (which was also aided by the surfactant) and pin holes developing in the deposit, promoted a more uniform current distribution, particularly in minimizing nodule formation at the high potential/current density regions round the edge of the electrodes, and gave an adherent copper deposit on the copper mesh cathode (Expament Ltd). The influence of the fluidized bed on the PbO_2 deposit morphology has been discussed elsewhere [25, 26]. Constant current in the range 1–40 A (50–2000 A m^{-2}) was applied from a 50 A/60 V power supply (Farnell Instruments Ltd) for a time determined by the charge theoretically required to produce a 0.1 mm thick deposit, assuming 100% current efficiency and a bulk density of 9.375 g cm^{-3}. Having formed the deposit at elevated electrolyte temperatures, the electrode was transferred rapidly to a large volume of preheated deionized water in which the electrode was allowed to cool slowly, to minimize thermal shock and the growth of internal stresses. Micrometer measurements of the electrode thickness indicated that the current efficiency was ~ 100%, which is in agreement with previous results [28]. More accurate determinations based on weight measurements, were not attempted as the Lacomit insulant tended to peel on removing the electrode from the cell, and at higher plating current densities PbO_2 nodules were lost from the electrode edges.

Appendix B

Determination of hypochlorite concentrations by automatic potentiometric titration

Automatic potentiometric titration with sodium arsenite solution potentially offers a quick and precise method for the determination of hypochlorite concentrations, with negligible interference from chloride, chlorate and chlorite.

A Pye autotitrator/delivery unit was used to add 0.01 mol dm^{-3} sodium arsenite from a 50 cm^3 burette to the hypochlorite sample or standard solution buffered with carbonate/bicarbonate, and platinum indicator/saturated calomel reference electrodes connected to a Pye model 291 pH meter were used to detect the end point.

This method was compared with two standard techniques [30] in which

i. the hypochlorite sample was treated with potassium iodide, acidified with acetic acid, and

the liberated iodine titrated with standard sodium thiosulphate solution:

$$ClO^- + 2I^- + 2H^+ \rightarrow Cl^- + I_2 + H_2O \quad (B1)$$

Acidification with acetic rather than hydrochloric acid, reduces interference from the slower oxidation of iodide by chlorate:

$$ClO_3^- + 6I^- \rightarrow Cl^- + 3I_2 + 3H_2O \quad (B2)$$

ii. an excess of standard sodium arsenite solution was added to the hypochlorite sample:

$$ClO^- + H_3AsO_3 \rightarrow H_3AsO_4 + Cl^- \quad (B3)$$

and the excess arsenite titrated against standard iodine solution.

From four sets of experiments, for hypochlorite concentrations of 50–500 mg dm^{-3}, the discrepancies between the three methods were:

(a) automatic potentiometric vs arsenite back titration	+ 0.73 to − 3.22%
(b) automatic potentiometric vs sodium thiosulphate titration	+ 0.63 to − 3.78%
(c) arsenite back titration vs thiosulphate titration	− 2.50 to + 1.89%

While the three methods do not compare very precisely with each other, the automatic titration is no worse than the other two.

References

[1] 'Local Generation and Use of Chlorine and Hypochlorite', SCI Electrochemical Technology Group Meeting, London, 14–16 October 1980.
[2] G. H. Kelsall, Electricity Council Research Centre Report N1059 (June 1977).
[3] A. T. Kuhn and R. B. Lartey, *Chem. Ing. Tech.* 47 (1975) 129.
[4] C.W. Tobias, *J. Electrochem. Soc.* **106** (1959) 333.
[5] Z. Nagy, *J. Appl. Electrochem.* 6 (1976) 171.
[6] N. Ibl and D. Landolt, *J. Electrochem. Soc.* **115** (1968) 713.
[7] L. Hammar and G. Wranglen, *Electrochim. Acta* 9 (1964) 1.
[8] A. T. Kuhn, H. Hamzah and G. C. S. Collins, *J. Chem. Tech. Biotechnol.* **30** (1980) 423.
[9] A. T. Kuhn and H. Hamzah, *Chem. Ing. Technol.* **52** (1980) 762.
[10] G. R. Heal, A. T. Kuhn and R. B. Lartey, *J. Electrochem. Soc.* **124** (1977) 1690.
[11] D. J. Pickett, 'Electrochemical Reactor Design', Elsevier, Amsterdam (1977).
[12] For example L. J. J. Janssen and J. G. Hoogland, *Electrochim. Acta* **15** (1970) 1013.
[13] N. Hackerman and C. D. Hall, *J. Electrochem. Soc.* **101** (1959) 827.
[14] N. T. Thomas and K. Nobe, *ibid.* **117** (1970) 622.
[15] D. T. Pickett and K. L. Ong. *Electrochim. Acta* **19** (1974) 875.
[16] R. E. De La Rue and C. W. Tobias, *J. Electrochem. Soc.* **106** (1959) 827.
[17] R. E. Meredith and C. W. Tobias, 'Advances in Electrochemistry and Electrochemical Engineering', Vol. 2. Interscience, New York (1962).
[18] J. Newman, 'Electrochemical Systems', Prentice-Hall, New York (1973).
[19] D. Jennings, A. T. Kuhn, J. B. Stepanek and R. Whitehead, *Electrochim. Acta* **20** (1975) 903.
[20] M. Morita, C. Iwakura and H. Tamura, *Electrochim. Acta* **22** (1977) 325.
[21] T. Loucka, *J. Appl. Electrochem.* 7 (1977) 211.
[22] M. Hayes and A. Kuhn, *ibid.* 8 (1978) 327.
[23] D. Gilroy, *ibid.* **12** (1982) 171.
[24] For example, P. Faber, 'Power Sources 4', Proceedings 8th International Symposium, Brighton (September 1972), (edited by D. H. Collins) Oriel Press, Newcastle, UK (1973).
[25] G. H. Kelsall and R. Stevens, Electricity Council Research Centre Report M1266 (July 1979).
[26] G. H. Kelsall, unpublished work.
[27] J. E. Bennett, Symposium on Electrochemical Reaction Engineering, Southampton University, (18–20 April 1979).
[28] G. H. Kelsall, Electricity Council Research Centre Report N1060 (June 1977).
[29] A. I. Vogel, 'Textbook of Quantitative Inorganic Analysis', 4th edn., Longmans, London (1978).
[30] M. Pourbaix, 'Atlas of Electrochemical Equilibria in Aqueous Solutions', National Association Corrosion Engineers, Houston, USA (1974).
[31] H. Vogt, *Electrochim. Acta* **26** (1981) 1311.